Phase Separation Kinetics of Polymer Dispersed Liquid Crystals Confined between Two Parallel Walls

Jianfeng Xia,[†,‡] Jun Wang,[†] Zhiqun Lin,*[,†] Feng Qiu,*[,‡] and Yuliang Yang[‡]

Department of Materials Science and Engineering, Iowa State University, Ames, Iowa 50011, and Department of Macromolecular Science, Fudan University, Shanghai 200433, China

Received December 19, 2005; Revised Manuscript Received January 15, 2006

ABSTRACT: The phase separation kinetics of polymer dispersed liquid crystals (PDLC) confined between two parallel, smooth walls are numerically studied for the first time. Only the two-dimensional (2D) system is considered for simplicity. The time evolutions of two order parameters (i.e., composition order parameter and orientational order parameter) are calculated by solving coupled time-dependent Ginzburg−Landau (TDGL) model C equations. The wall surface effect is weaker when the thermal quench is deeper. The ordering of LC is found to be accelerated as the external confinement is enhanced (i.e., reduced separation distance between two walls). The results presented in the study will provide insights into the experiments on the control of LC domain morphologies in the mixture of polymer/LC under nanoscopic confinement.

I. Introduction

The mixtures of polymer and low-molecular-weight liquid crystal (LC) are of immense interest scientifically and technologically due to their potential applications in the area of electrooptical devices and flat panel displays, etc.[1] Polymer/LC mixtures can be divided into several categories, including polymer stabilized liquid crystals (PSLC)[2−7] and polymer dispersed liquid crystals (PDLC).[8−16] A new class of PDLC is the holographically formed PDLC (i.e., H-PDLC) produced by pattern photopolymerization using UV irradiation.[17−24] The simplest way of preparing PDLC materials is through the thermal quench of a homogeneous mixture of LC and polymer. The performance of PDLC strongly depends on the final morphology of the dispersed LC domain in polymer matrix. The size, shape, and distribution of LC domains are generally not only dictated by thermodynamic phase equilibria but also strongly dependent on phase separation kinetics and anisotropic ordering of LC as most polymer systems hardly reach a thermodynamic equilibrium state.[25] Thus, the fundamental understanding of the phase equilibrium and phase separation kinetics of mixtures of polymer/LC is of crucial importance for optimizing the performance of PDLC materials. On the other hand, the dynamics of spinodal decomposition in a mixture containing anisotropic moieties (e.g., LC) is also an interesting theme for the study of complex fluids or soft matters.

Both experimental[8−16] and theoretical[8,9,12,14,26,27] studies on the phase equilibrium of PDLC systems have been reported in recent years. The Flory−Huggins lattice theory of polymer mixture[28] and the Maier−Saupe[29,30] or the Lebwohl−Lasher[31,32] models of nematogens were combined to predict the phase diagram of polymer/nematic LC mixtures that consists of isotropic, liquid−liquid, isotropic−nematic, and pure nematic regions.[8−13,15,16,33,34] The theoretical calculations agreed well with experimental observations in various polymer/LC mixture systems.[1,8−13] The time-dependent Ginzburg−Landau (TDGL) equations (model C)[35] that couple the local composition order parameter, ϕ, with the nematic order parameter of LC, either scalar[25,33,36] or tensor,[14,34,37−41] have been employed to simulate the morphological evolutions. The morphologies depend on the region in which the mixture is quenched[8−13,15,16,33,34] (i.e., in the isotropic spinodal region or anisotropic spinodal region (Figure 1)). For example, an interesting pattern constituting concentric domains was obtained when the mixture was quenched into a shallow spinodal region which was close to the nematic−isotropic (NI) transition line.[14] The polymer-rich phase was found to form an interconnected domain due to viscoelastic effects, even when the polymer component was minority.[39] It has been demonstrated that the nematohydrodynamic effects not only accelerated the LC domain growth but also led to the breakdown of the morphological symmetry of the two phases.[34]

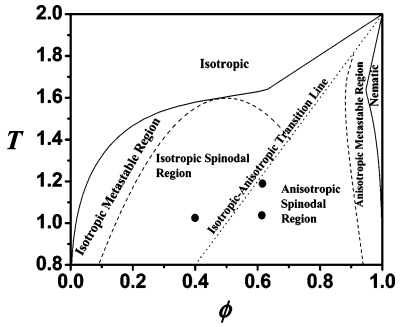

Figure 1. Phase diagram of polymer/LC binary mixture with $\alpha = 1.0$, $T_{NI} = 2.0$, and $\chi_0 = 2.8$. The solid line refers to the binodal curve. The dash line is the spinodal curve. The dotted line represents the isotropic to anisotropic (i.e., nematic in the present study) transition. The solid circles indicate the volume fraction and the corresponding temperature at which the mixture is quenched from homogeneous isotropic state.

Despite the technical importance, the comprehensive understanding of the phase separation kinetics in LC/polymer mixtures, both experimentally[13,14,25,42] and theoretically,[14,25,27,33,38] is still far from complete. In particular, to the best of our knowledge, no theoretical and experimental efforts concerned on the surface and finite size effects on the phase separation kinetics of a PDLC system in confined geometries have been made. This contrasts significantly with the intensive studies that have been devoted to investigate LC solely confined by smooth walls,[43] in nanopores,[44−48] and in a prefabricated polymer

† Iowa State University.
‡ Fudan University.
* To whom correspondence should be addressed. E-mail: zqlin@iastate.edu and fengqiu@fudan.edu.cn.

10.1021/ma0527045 CCC: $33.50
Published on Web 02/15/2006

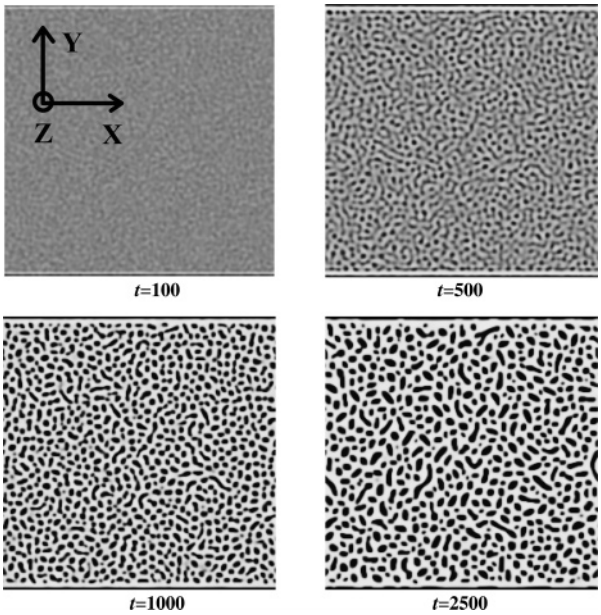

Figure 2. Snapshots of the morphologies of PDLC confined between two solid surfaces after quenched to $T = 1.0$. The black and white correspond the LC-rich phase and the polymer-rich phase, respectively. The wall surfaces adsorb LCs. The initial volume fraction of LC, $\phi_{ini} = 0.4$. The simulation is carried out in 256×256 lattice sites.

template,[49] in which surface and finite size effects have been shown to exert profound influences on the kinetics of LC.

In this paper, we employ the coupled time-dependent Ginzburg−Landau (TDGL) equations (model C)[35] for the local volume fraction (i.e., composition order parameter), ϕ, with the nematic tensor order parameter, Q, to explore, for the first time, the emergence of nematic ordering of LCs and the phase separation kinetics during thermally induced phase separation in a PDLC system confined between two parallel, smooth, and impenetrable walls. We show that the surface effect becomes weaker when the thermal quench is deeper. The isotropic to nematic transition of LC is enhanced as the distance between two walls reduced. The paper is organized as follows. In section II we describe the model and simulation method. We then present and discuss the interesting features of the phase separation kinetics of PDLC and orientational order parameter of LC under external confinement in section III, followed by conclusions in section IV.

II. Model and Simulation Method

II.1. Free Energy of Polymer/LC Mixture. A mixture of flexible polymer and LCs is confined between two parallel, smooth, and impenetrable walls that locate at the Y direction in the coordinate illustrated in Figure 2. Only the two-dimensional (2D) system is considered for simplicity. The mixture can be described by a conserved order parameter, volume fraction of liquid crystal, ϕ, and a nonconserved traceless symmetric tensor orientational order parameter of LC, Q_{ij}, defined as[14,36,37,47]

$$Q_{ij}(r) = \frac{3}{2}S(r)\left(n_i(r)n_j(r) - \frac{1}{3}\delta_{ij}\right) \tag{1}$$

where $i, j = X, Y, Z$ represent the components along three orthogonal coordinate axes.[40] The Z direction is parallel to the wall surfaces (Figure 2). $S(r)$ is the scalar orientational order parameter, and $n(r)$ is a local director field.[40] Q_{ZZ}, Q_{XZ}, and Q_{YZ} are chosen to be independent variables in the simulation.[39]

$$S(r) = \frac{2}{3}\left(\frac{Q_{zz}(r)}{n_z(r)^2 - {}^1/_3}\right) \tag{2}$$

for $Q_{ZZ}(r) \neq 0$. Otherwise[39]

$$S(r) = \sqrt{2(Q_{xz}(r)^2 + Q_{yz}(r)^2)} \tag{3}$$

The free energy of the system contains two parts, i.e., the bulk free energy and surface free energy resulting from the external confinement effect

$$F[\phi,Q_{ij}] = F_{bulk}[\phi,Q_{ij}] + F_{sur}[\phi,Q_{ij}] \tag{4}$$

The bulk free energy, F_{bulk}, is given by the integration of the local free energy density[14,39]

$$F_{bulk}[\phi,Q_{ij}] = \int dr \left[f(\phi,Q_{ij}) + \frac{1}{2}(\nabla\phi)^2 + \frac{c_1}{2}(\nabla_k Q_{ij})(\nabla_k Q_{ij}) + \frac{c_2}{2}(\nabla_i\phi)(\nabla_j\phi)Q_{ij} \right] \tag{5}$$

where F_{bulk} and the bulk free energy density, f, are dimensionless quantities divided by k_BT. c_1 is phenomenological coefficient arising from the elastic energy of LCs; c_2 is also a phenomenological coefficient specifying the orientation of LC at the interface between polymer-rich phase and LC-rich phase. f is given as[14]

$$f(\phi,Q_{ij}) = \alpha(1-\phi)\ln(1-\phi) + \phi\ln\phi + \chi_{LP}\phi(1-\phi) + [T - (T_{NI} - c_3(1-\phi))](TrQ^2) + C(TrQ^2)^2 \tag{6}$$

where the constant α is defined as $\alpha = n_L/n_P$, where n_L and n_P are the molecular weights of LC and polymer, respectively. χ_{LP} is the Flory interaction parameter between polymer and LCs and assumed to be inversely proportional to the temperature T

$$\chi_{LP} = \frac{\chi_0}{T} \tag{7}$$

where χ_0 is a positive constant. T_{NI} is the nematic−isotropic transition temperature in the absence of polymer. c_3 and C are positive constants. Since a uniaxial LC is considered for simplicity, the higher-order term of Landau−de Gennes expansion of orientational order parameter in f is neglected.[14]

The surface energy, F_{sur}, has two contributions: the first origins from the affinities of the surface for polymer or LC, which can be expressed as a long-range surface potential[50]

$$F_{sur\_aff}[\phi(r)] = \int dr\, V(r)\,\phi(r) \tag{8}$$

It depends solely on the distance from the interacting wall and is given by[50]

$$V(r) = \begin{cases} -\dfrac{\sigma}{d^{p+1}} & r \neq r_{sur} \\ -\sigma & r = r_{sur} \end{cases} \tag{9}$$

where d is the distance away from the wall. The values of $\sigma = 0.4$ and $p = 2$ are taken in the simulation.[51,52] The second results from the surface anchoring effect on orientation of LCs[53]

$$F_{sur\_anc} = \int dr\, f_s[Q_{ij},r] \tag{10}$$

where $f_s[Q_{ij},r]$ is the local density of interaction energy. However, this term is ignored in the simulation because the

values of n_X and n_Y cannot be determined uniquely when LC locates in the $X-Y$ plane (i.e., at $n_Z = 0$).[39] Moreover, we are interested in the situation in which no anchoring effect on the LCs is imposed by the wall surfaces[47] (i.e., zero anchoring instead of homogeneous and/or homeotropic anchoring).

The typical phase diagram of polymer/LC binary mixture in bulk, that is, in the absence of the external confinement, calculated by combining the Flory−Huggins model[28] for an isotropic polymer mixture and the Lebwohl−Lasher model[31,32] for the nematogens is presented in Figure 1. For details of calculation, one can refer to our previous papers.[15,16,33,42] It is seen that the phase diagram is highly asymmetric, and there exists a narrow nematic phase region when the volume fraction of LC, ϕ, is high. There are two spinodal regions, i.e., an isotropic spinodal region and an anisotropic (i.e., nematic) spinodal region, which are separated by an anisotropic−isotropic (N−I) transition line.

II.2. Kinetic Model. The time evolutions of composition order parameter of LC, ϕ, and orientational order parameter, Q, can be described by the coupled time-dependent Ginzburg−Landau (TDGL) equations (model C).

$$\frac{\partial\phi(r,t)}{\partial t} = M_\phi \nabla^2 \frac{\delta F[\phi, Q_{ij}]}{\delta\phi(r)} + \eta \tag{11}$$

$$\frac{\partial Q_{ij}(r,t)}{\partial t} = -M_S\left[\frac{\delta F[\phi, Q_{ij}]}{\delta Q_{ij}(r)} + \lambda\delta_{ij}\right] + \eta_{ij} \tag{12}$$

where M_ϕ and M_S are the mobility coefficients that depend on the molecular weights of polymer and LC as well as the local composition order parameter, ϕ, and orientational order parameter, Q. For simplicity, they are assumed to be constants in the simulation as employed by Motoyama et al.[14] Equation 11 is a conserved diffusion equation where the thermodynamic force driven flux is given by the chemical potential $\mu = \delta F/\delta\phi$. Equation 12 is a nonconserved orientational order parameter equation. The Lagrange multiplier λ is chosen to ensure the traceless tensor condition Tr $Q = 0$. It should be noted that $n_X^2 + n_Y^2 + n_Z^2 = 1$ has been confirmed in the simulation. In other words, Tr $Q = 0$ is satisfied. The last terms in eqs 11 and 12 are the thermal random noises which can be described by the fluctuation dissipation relations[14]

$$\langle\eta(r,t),\eta(r',t')\rangle = -2M_\phi\nabla^2\delta(r-r')\delta(t-t') \tag{13}$$

$$\langle\eta_{ij}(r,t),\eta_{kl}(r',t')\rangle = -2M_S\delta_{ik}\delta_{jl}\delta(r-r')\delta(t-t') \tag{14}$$

Substituting eqs 4−6, 8, and 9 into eqs 11 and 12, the kinetics equations for ϕ and Q can be obtained

$$\frac{\partial\phi(r,t)}{\partial t} = \nabla^2[\alpha(\ln[1-\phi(r)]+1) - (\ln[\phi(r)]+1) + \chi_{LP}(1-2\phi(r)) - \nabla^2\phi(r) - c_2\nabla_i\{(\nabla_j\phi(r))Q_{ij}(r)\} + c_3 \text{Tr } Q^2 + V(r)] + \eta \tag{15}$$

$$\frac{\partial Q_{ij}(r,t)}{\partial t} = c_1\nabla^2 Q_{ij}(r) - \frac{c_2}{2}(\nabla_i\phi(r))(\nabla_j\phi(r)) + \frac{c_2}{6}(\nabla\phi(r))^2\delta_{ij} - \{2[T - (T_{NI} - c_3(1-\phi(r)))] + 4C(\text{Tr } Q^2)\}Q_{ij}(r) + \lambda\delta_{ij} + \eta_{ij} \tag{16}$$

Equations 15 and 16 are solved numerically in two-dimensional square lattice ($X \times Y = N \times N$). The periodic boundary condition is applied in the X direction (Figure 2). To ensure that there is no mass transport at the two wall surfaces since PDLC cannot penetrate the hard walls (the position of two wall surfaces are set as $Y = 0$ and $Y = N + 1$),[50] the following boundary condition is employed for the conserved composition order parameter, ϕ

$$\frac{\partial\mu}{\partial Y} = 0 \tag{17}$$

For nonconserved orientational order parameter, Q, the Neumann boundary condition is used, assuming that the wall surfaces impose no effect on the orientation of LC (i.e., zero anchoring assumption).[47]

$$Q(x, 0, t) = Q(x, 1, t)$$
$$Q(x, N+1, t) = Q(x, N, t) \tag{18}$$

The following parameters are set in the simulation: $c_1 = 1.0$, $c_2 = -1.0$, $c_3 = 2.0$, $T = 1.0$, $T_{NI} = 2.0$, $\chi_0 = 2.8$, $C = 1.0$, and $\alpha = 1.0$.[14] The initial local LC volume fraction and the initial scalar order parameter are assumed to distribute uniformly around their average values (i.e., $\langle\phi_{ini}\rangle = 0.4$ (or 0.6) and $\langle S\rangle = 0.01$). The director $n(r)$ takes a random configuration. An explicit method for temporal steps and a central difference scheme for spatial steps with a periodic boundary condition in the X direction are used. The discretized space and time are $\Delta X(Y) = 1.0$ and $\Delta t = 0.001$, respectively. The thermal random noises were neglected in the calculations since they have no significant effect on the last stage phase separation kinetics.[14,54,55]

III. Results and Discussion

1. Surface Effects on the Ordering of Liquid Crystals. Figure 2 shows the spatial−temporal evolutions of morphologies of PDLC confined between two solid walls at $\phi_{ini} = 0.4$ after quenched to $T = 1.0$, i.e., in isotropic spinodal region (Figure 1). The black and the white represent the LC-rich phase and the polymer-rich phase, respectively. The LC domains are dispersed in the polymer matrix. Although interfacial interactions between the LCs and walls are expected to play an important role in the alignment and orientational ordering of LCs, the wall surfaces are only considered to selectively adsorb LCs. The zero anchoring at the walls is assumed in the simulation. A LC-rich layer forming at two wall surfaces is clearly evident (Figure 2). Similar phenomena have been observed in the thin film of a polymer blend[56] as well as the diblock copolymer[50] when they were confined between two slabs. A strong surface-induced segregation was obtained in the diblock copolymer.[50] It has been demonstrated that when small molecular weight LC 5CB was restricted in a silica aerogel of continuous pore structure, a layer of 5CB was found to form at the nontreated silica internal wall surface as probed by NMR.[45]

The time evolution of the corresponding LC director configuration in 64×64 lattice sites is illustrated in Figure 3. At the very early stage of the phase separation, the polymer and LC are still miscible. No ordered LC at $t = 100$ is seen except the regions at the wall surfaces.[55] It can be seen that LC molecules align to some angles to the walls and the directors gradually turn away from the plane (i.e., the rods become shorter as LC molecules are gradually away from the walls). The ordering of LC at the walls is caused by surface-induced phase separation that drives the LC to enrich at the walls at the temperature below T_{NI}. The director of LCs would tend to adopt an optimal state to balance all elastic energies (i.e., splay, twist,

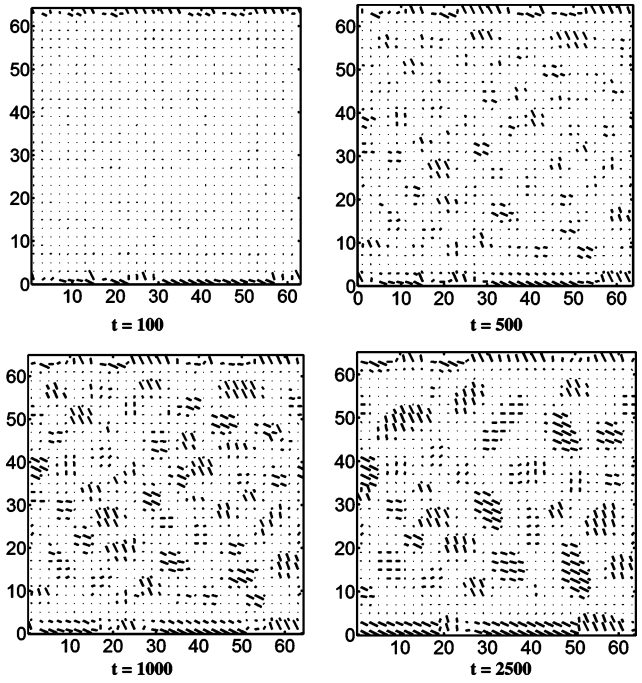

Figure 3. Snapshots of the director configurations of LC ($\phi_{ini} = 0.4$) for PDLC confined between two solid walls after quenched to $T = 1.0$. The wall surfaces adsorb LCs. The lattice size is 64 × 64.

and bend).[53] A spatial variation of the director is, thus, inevitably expected near the wall surfaces. This causes a nonzero tilt angle.[53]

The director configurations inside a LC-rich domain dictate its shape. As time progresses, rather than the circular shape, the LCs domains are observed to be elongated due to a negative constant $c_2 = -1.0$ employed in the simulation.[14] The individual LC molecule is seen to align preferentially perpendicular to the polymer/LC interface, especially at $t = 2500$, as a direct consequence of the reduction of the interfacial interaction between polymer and LC through increasing the interface area of the perpendicular orientation.[14]

In the simulation, the relevant variables are the local volume fraction of LC and the order parameter of LC. The distribution of volume fraction of LC, ϕ in $X-Y$ plane at $t = 100$ (Figure 3) is depicted in Figure 4a. The ϕ at the walls is ~0.8, greater than 0.5. The nematic to isotropic transition of LC takes place at $T = 1.0$ and $\phi = 0.5$ (Figure 1). Therefore, it is clear that the polymer/LC mixture has phase separated at the walls. However, the average ϕ in away-from-wall regions is ~0.4, signifying surface-induced ordering of LC occurs earlier than those in the regions away from the walls. This is manifested in a larger value of the scalar orientational order parameter S at the walls at $t = 100$ ($S = \sim 0.05$) as shown in the inset in Figure 4b. As time progresses, a thicker layer of LC-rich domain at the wall surface is formed as is evidenced in Figure 2 (i.e., thicker black stripes at both top and bottom walls). In other words, more LC molecules are seen to adsorb at the walls. Accordingly, the surface ordering of LC becomes significant and reaches a constant value ~0.55 after $t = 500$ (Figure 4b). However, the ordering away from wall surfaces is observed to increase gradually from 0.1 at $Y = 8$, $t = 500$ to 0.4 at $Y = 9$, $t = 1000$ to 0.45 at $Y = 10$, $t = 2500$. It is interesting to observe a surface-induced ordering of LC for a confined PDLC film. This is analogous to the surface-induced segregations in diblock copolymer thin films.[50]

2. Quenching Depth Effects: Shallow vs Deep Quench. Figures 5 and 6 illustrate the spatial−temporal evolutions of

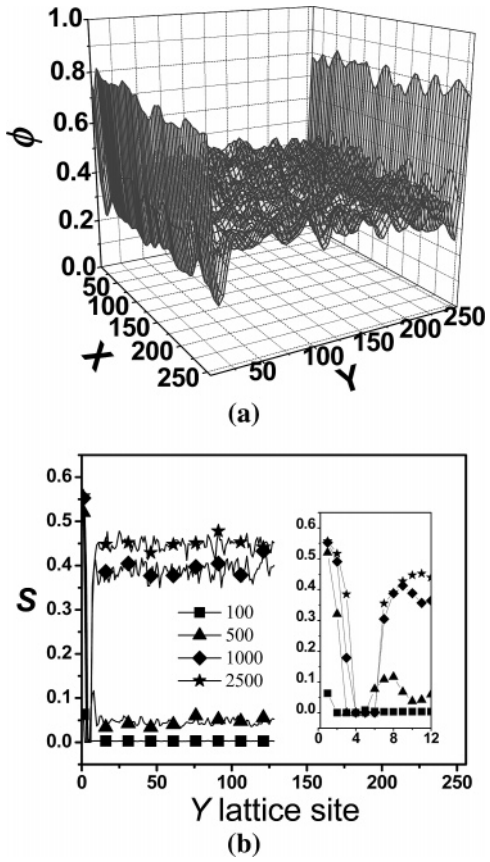

Figure 4. (a) Spatial distribution of ϕ in 2D space (i.e., $X-Y$ plane) at $t = 100$. (b) Spatial distribution of average scalar orientational order parameter in Y direction at different time. The distribution of the first 12 lattice sites is shown in the inset. The wall surfaces adsorb LCs. The initial volume fraction of LC, $\phi_{ini} = 0.4$. $T = 1.0$.

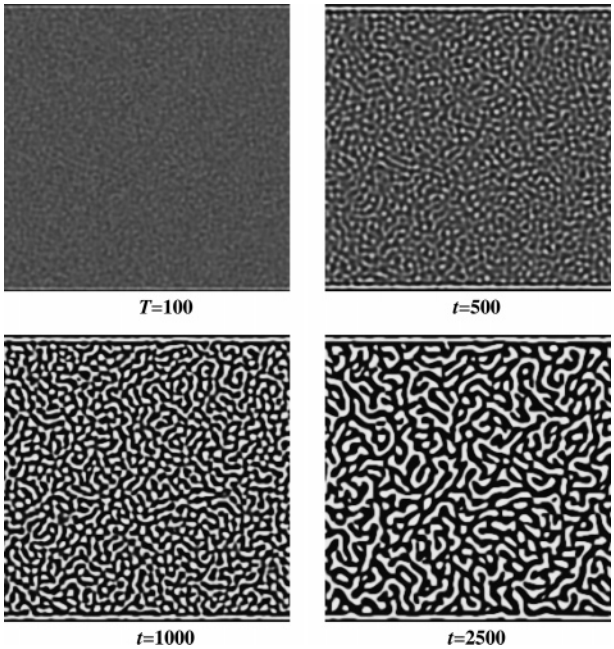

Figure 5. Snapshots of the morphologies of PDLC confined between two solid surfaces after quenched to $T = 1.0$ (deep quench). The black and white correspond the LC-rich phase and the polymer-rich phase, respectively. The wall surfaces adsorb LCs. The initial volume fraction of LC, $\phi_{ini} = 0.6$. The simulation is carried out in 256 × 256 lattice sites.

morphologies of confined PDLC with initial volume fraction of LC, $\phi_{ini} = 0.6$ after quenched to anisotropic spinodal region

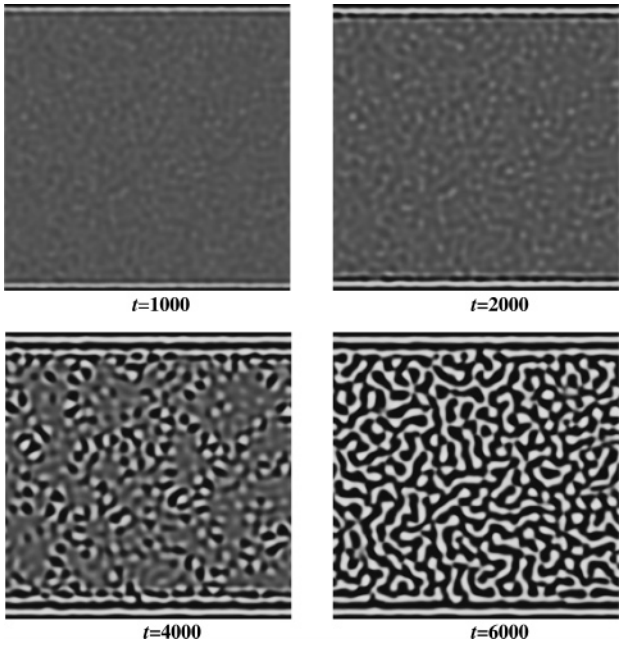

Figure 6. Snapshots of the morphologies of PDLC confined between two solid surfaces after quenched to $T = 1.2$ (shallow quench). The black and white correspond the LC-rich phase and the polymer-rich phase, respectively. The wall surfaces adsorb LCs. The initial volume fraction of LC, $\phi_{ini} = 0.6$. The simulation is carried out in 256×256 lattice sites.

(Figure 1). The nematic to isotropic transition line is given by $T/T_{NI} = \phi$.[57] The quench depth in Figure 5 (i.e., $T = 1.0$; deep quench) is larger than that in Figure 6 (i.e., $T = 1.2$; shallow quench). At the same initial volume fraction the deeper quench yields smaller domain size as is evidenced in Figure 5.[58] The polymer domains dispersed in LC matrix are clearly evident at $t = 1000$ under deep quench (Figure 5). This contrasts dramatically with the one undergoing shallow quench at the same time, where the mixture is still at the early stage of spinodal decomposition (Figure 6). The surface-induced spinodal wavelength undergoing deep quench (Figure 5) is smaller than that via shallow quench (Figure 6), which agrees well with the surface-directed spinodal decomposition of mixtures of PEP/d-PEP studied using forward−recoil spectrometry by Kramer et al.[59] It is noteworthy that the phase separation and nematic ordering of LC occur simultaneously under deep quench, while the phase separation is seen to proceed ($t = 2000$) prior to the ordering of LC becoming significant under shallow quench ($t = 4000$, represented as brighter dark domains (i.e., LC) in the hazy background in Figure 6).

Of particular interest is that two distinct alternative layers of LC and polymer are seen to propagate from the wall surfaces (Figure 6). However, only one layer of LC and polymer is detected under deep quench (Figure 5). This can be rationalized as follows. The driving force for the spinodal decomposition is low for $T = 1.2$ (i.e., shallow quench) so that the phase separation cannot exert an enough force to overcome the surface effect to destabilize the adsorption layers. Thus, more layers are formed at the wall surfaces. However, for $T = 1.0$ (i.e., deep quench) the larger force resulting from larger temperature difference drives a stronger phase separation, which, in turn, enables the disruption of the second to the last layers of LC and polymer. As a result, only a monolayer of LC is adsorbed on the walls, followed by a layer of polymer.

3. Finite Size Effects on the Ordering of LC. Finite size effects have been shown to exert pronounced influences on the kinetics of LC,[44−48] the phase separation of polymer mixtures,[56] and the ordering of block copolymers.[50,60] Figures 7 and 8 show the morphologies of confined PDLC after reaching static state (see the plateaus of ϕ and S in Figure 9). The mixture at $\phi_{ini} = 0.6$ is thermally quenched to $T = 1.0$. The wall surface plays an important role in determining the final static morphologies as the separation distance between two walls reduces. A salient difference between morphologies undergoing deep and shallow quench is that, when the characteristic wavelength $\lambda = 2\pi/q$ of spinodal decomposition and the size of external confinement become comparable, only a layer of LC and polymer results in when the driving force for the phase separation is stronger under deep quench (the image of 256×32 in Figure 7), while periodic structures are achieved when the surface effect is so significant that it dominates over the phase separation kinetics (the image of 256×32 in Figure 8). The latter observation may offer a strategy to produce patterned ultrathin PDLC films with enhanced optical performance and devices[61] based upon them without the use of UV irradiation for pattern photopolymerization as in the fabrication of H-PDLC.[17−21]

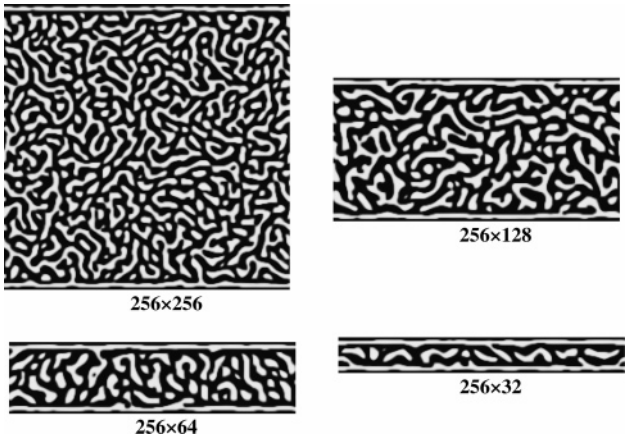

Figure 7. Finite size effects on the final static morphologies of PDLC. The initial volume fraction of LC, $\phi_{ini} = 0.6$. The simulations are performed using the same parameters as those in Figure 5, except the changes of the lattice size in Y axis. $T = 1.0$.

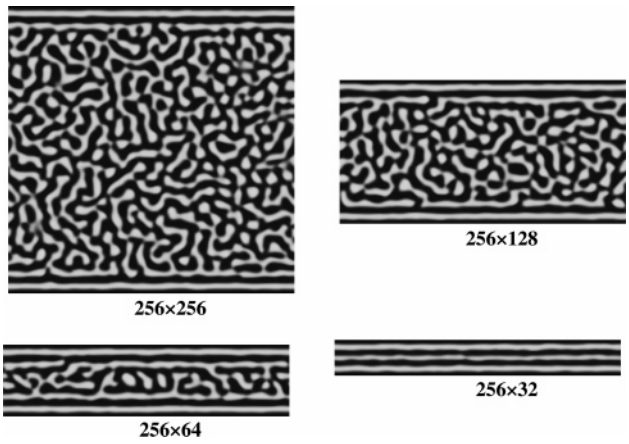

Figure 8. Confinement effects on the final static morphologies of PDLC. The initial volume fraction of LC, $\phi_{ini} = 0.6$. The simulations are performed using the same parameters as those in Figure 6, except the changes of the lattice size in Y axis. $T = 1.2$.

The average order parameters, both the scalar nematic order parameter S and the compositional order parameters, ϕ_P and ϕ, in LC-rich domains, as a function of time are shown in Figure 9. For PDLC confined between two walls that are separated by 256 lattice sites, the S gradually increases as time progresses and reaches a plateau at $t = \sim 1000$ (squares in Figure 9a). In

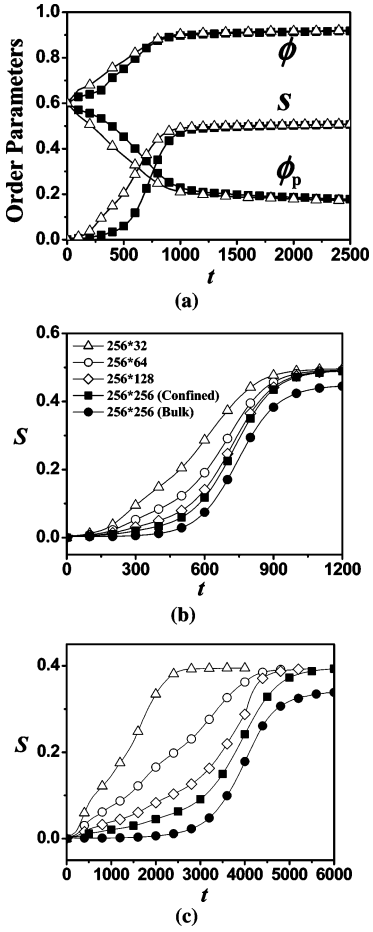

Figure 9. Time evolution of the average order parameters: both scalar nematic order parameter S (a−c) and compositional order parameter ϕ_P and ϕ in LC-rich domains (a) in the confined PDLC. The initial volume fraction of LC, $\phi_{ini} = 0.6$. (a, b) $T = 1.0$; (c) $T = 1.2$.

the meantime ϕ follows the same trend and yields a constant value of 0.84 after $t = 1000$. The converse is observed for ϕ_P (the volume fraction of the polymer) as a result that the polymers are repelled from the LC-rich domains with time as the isotropic to nematic transition of LC takes place. It is clear that the phase separation of PDLC confined between two walls that are separated by 32 lattice sites (triangles in Figure 9a) proceeds more aggressively than that confined between 256-lattice-site walls. To explore the finite size effects, the S for PDLC phase-separating at the different wall distance as well as in bulk (i.e., no confinement) are calculated while keeping the other parameters fixed (Figure 9b,c). Under deep quench ($T = 1.0$), S levels off at a greater value (∼0.5) under confinement than that in bulk (∼0.43) (Figure 9b). Although the plateau values of S do not differ much under different confinements, the isotropic to nematic ordering transition time, t_{tran}, defined as the peak observed in the first derivative of the $S \sim t$ curve, is shorter as the external confinement is intensified (i.e., decreased surface separation of the walls). For example, t_{tran} in the case of a surface distance of 32 lattice sites is ∼590, while t_{tran} is ∼730 for a surface distance of 256 lattice sites. The finite size effect accelerates the phase separation (Figure 9a), which, in turn, leads to a faster isotropic to nematic ordering transition in the PDLC. A similar trend is observed for the PDLC undergoing shallow quench ($T = 1.2$) (Figure 9c). In contrast to the case of deep quench, the larger difference in t_{tran} can be seen as the imposed confinement is strengthened, e.g., t_{tran} ∼1610 (32 lattices) vs t_{tran} ∼4000 (256 lattices), nearly 2.5 times faster in the case of 32 lattices. These results point to a simple route by which the faster switch speed of LC in PDLC can be easily and rapidly implemented by reducing the separation distance of two walls.

IV. Conclusion

The phase separation kinetics of polymer dispersed liquid crystals (PDLC) confined between two parallel hard walls are numerically studied.The spatial−temporal evolution of both conserved compositional order parameter and nonconserved orientational order parameter during the spinodal decomposition are calculated. The tensorial nature of orientational order parameter is considered. A surface-induced ordering transition of LC at the walls is observed, and it is faster than that in the away-from-surface regions due to the fact that the walls adsorb LCs. Periodic structures are achieved when the surface effect dominates over the phase separation kinetics. The phase separation kinetics of PDLC as well as the nematic odering transition are accelerated as the external confinement is intensified. The present results may provide insights into producing patterned ultrathin PDLC films with enhanced optical performance (e.g., faster switching speed) and devices based upon them. The simulations are performed in two dimensions. We envision that the three-dimensional calculations may carry more interesting features because of the presence of long-range orientational correlations in neighboring LC domains.

Acknowledgment. This work is supported by the American Chemical Society Petroleum Research Fund (Grant 42825-G7).

References and Notes

(1) Mucha, M. *Prog. Polym. Sci.* **2003**, *28*, 837.
(2) Guymon, C. A.; Dougan, L. A.; Martens, P. J.; Clark, N. A.; Walba, D. M.; Bowman, C. N. *Chem. Mater.* **1998**, *10*, 2378.
(3) Guymon, C. A.; Hoggan, E. N.; Clark, N. A.; Rieker, T. P.; Walba, D. M.; Bowman, C. N. *Science* **1997**, *275*, 57.
(4) Lester, C. L.; Smith, S. M.; Colson, C. D.; Guymon, C. A. *Chem. Mater.* **2003**, *15*, 3376.
(5) Lester, C. L.; Smith, S. M.; Jarrett, W. L.; Guymon, C. A. *Langmuir* **2003**, *19*, 9466.
(6) McCormick, D. T.; Chavers, R.; Guymon, C. A. *Macromolecules* **2001**, *34*, 6929.
(7) Kossyrev, P.; Sousa, M. E.; Crawford, G. P. *Adv. Funct. Mater.* **2004**, *14*, 1227.
(8) Shen, C.; Kyu, T. *Chem. Phys.* **1995**, *102*, 556.
(9) Chiu, H. W.; Kyu, T. *J. Chem. Phys.* **1995**, *103*, 7471.
(10) Nwabunma, D.; Kim, K. J.; Lin, Y. H.; Chien, L. C.; Kyu, T. *Macromolecules* **1998**, *31*, 6806.
(11) Nwabunma, D.; Kyu, T. *Macromolecules* **1999**, *32*, 664.
(12) Roussel, F.; Buisine, J.; Maschke, U.; Coqueret, X.; Benmouna, F. *Phys. Rev. E* **2000**, *62*, 2310.
(13) Nwabunma, D.; Chiu, H.; Kyu, T. *Macromolecules* **2000**, *33*, 1416.
(14) Motoyama, M.; Nakazawa, H.; Ohta, T.; Fujinami, S.; Nakada, H.; Hayashi, M.; Aizawa, M. *Comput. Theor. Polym. Sci.* **2000**, *10*, 287.
(15) Zhang, H.; Lin, Z.; Yan, D.; Yang, Y. *Sci. China Ser. B* **1997**, *40* (2), 128.
(16) Lin, Z.; Zhang, H.; Yang, Y. *Phys. Rev. E* **1998**, *58*, 5867.
(17) De Sarkar, M.; Gill, N. L.; Whitehead, J. B.; Crawford, G. P. *Macromolecules* **2003**, *36*, 630.
(18) Kyu, T.; Nwabunma, D.; Chiu, H. W. *Phys. Rev. E* **2001**, *63*, 061802.
(19) Kyu, T.; Nwabunma, D. *Macromolecules* **2001**, *34*, 9168.
(20) Pogue, R. T.; Sutherland, R. L.; Schmitt, M. G.; Natarajan, L. V.; Siwecki, S. A.; Tondiglia, V. P.; Bunning, T. J. *Appl. Spectrosc.* **2000**, *54*, 1.
(21) Vaia, R. A.; Tomlin, D. W.; Schulte, M. D.; Bunning, T. J. *Polymer* **2001**, *42*, 1055.
(22) Meng, S.; Kyu, T.; Natarajan, L. V.; Tondiglia, V. P.; Sutherland, R. L.; Bunning, T. J. *Macromolecules* **2005**, *38*, 4844.
(23) Qi, J.; Li, L. L.; Sarkar, M. D.; Crawford, G. P. *J. Appl. Phys.* **2004**, *96*, 2443.
(24) Qi, J.; Sousa, M. E.; Fontecchio, A. K.; Crawford, G. P. *Appl. Phys. Lett.* **2003**, *82*, 1652.
(25) Chiu, H. W.; Kyu, T. *J. Chem. Phys.* **1999**, *110*, 5998.
(26) Kyu, T.; Chiu, H. W. *Phys. Rev. E* **1996**, *53*, 3618.
(27) Muratova, C. B.; Weinan, E. *J. Chem. Phys.* **2002**, *116*, 4723.

(28) Flory, P. J. *Principles of Polymer Chemistry*; Cornell University Press: Ithaca, NY, 1953.
(29) Maier, W.; Saupe, A. *Teil I. Z. Naturforsch.* **1959**, *14a*, 882.
(30) Maier, W.; Saupe, A. *Teil I. Z. Naturforsch.* **1960**, *15a*, 287.
(31) Lasher, G. *Phys. Rev. A.* **1972**, *5*, 1350.
(32) Lebwohl, P. A.; Lasher, G. *Phys. Rev. A* **1972**, *6*, 426.
(33) Lin, Z.; Zhang, H.; Yang, Y. *Macromol. Theory Simul.* **1997**, *6*, 1153.
(34) Araki, T.; Tanaka, H. *Phys. Rev. Lett.* **2004**, *93*, 015702.
(35) Hohenberg, P. C.; Halperin, B. I. *Rev. Mod. Phys.* **1977**, *49*, 435.
(36) Nwabunma, D.; Chiu, H. W.; Kyu, T. *J. Chem. Phys.* **2000**, *113*, 6429.
(37) Langer, S. A.; Glotzer, S. C. *Physica A* **1997**, *239*, 358.
(38) Liu, A.; Fredrickson, G. H. *Macromolecules* **1996**, *29*, 8000.
(39) Nakazawa, H.; Fujinami, S.; Motoyama, M.; Ohta, T.; Araki, T.; Tanaka, H.; Fujisawa, T.; Nakada, H.; Hayashi, M.; Aizawa, M. *Comput. Theor. Polym. Sci.* **2001**, *11*, 445.
(40) Matsuyama, A.; Evans, R. M. L.; Cates, M. E. *Phys. Rev. E* **2000**, *61*, 2977.
(41) Das, S. K.; Reya, A. D. *J. Chem. Phys.* **2004**, *121*, 9733.
(42) Lin, Z.; Zhang, H.; Yang, Y. *Macromol. Chem. Phys.* **1999**, *200*, 943.
(43) Steuer, H.; Hess, S.; Schoen, M. *Phys. Rev. E* **2004**, *69*, 031708.
(44) Massalska-Arodz, M.; Gorbachev, V. Y.; Krawczyk, J.; Hartmann, L.; Kremer, F. *J. Phys.: Condens. Matter* **2002**, *14*, 8435.
(45) Kralj, S.; Lahajnar, G.; Zidansek, A.; Vrbancic-Kopac, N.; Vilfan, M.; Blinc, R.; Kosec, M. *Phys. Rev. E* **1993**, *48*, 340.
(46) Steinhart, M.; Zimmermann, S.; Goring, P.; Schaper, A. K.; Gosele, U.; Weder, C.; Wendorff, J. H. *Nano Lett.* **2005**, *5*, 429.
(47) Bhattacharya, A.; Rao, M.; Chakrabarti, A. *Phys. Rev. E* **1996**, *53*, 4899.
(48) Crawford, G. P.; Ondris-Crawford, R. J.; Doane, J. W. *Phys. Rev. E* **1996**, *53*, 3647.
(49) Luther, B. J.; Springer, G. H.; Higgins, D. A. *Chem. Mater.* **2001**, *13*, 2281.
(50) Brown, G.; Chakrabarti, A. *J. Chem. Phys.* **1994**, *101*, 3310.
(51) Brown, G.; Chakrabarti, A. *Phys. Rev. A* **1992**, *46*, 4829.
(52) Lipowsky, R. *J. Phys. A* **1985**, *18*, L585.
(53) Qian, T. Z.; Sheng, P. *Phys. Rev. E* **1997**, *55*, 7111.
(54) Meng, S.; Nanjundiah, K.; Kyu, T.; Natarajan, L. V.; Tongdiglia, V. P.; Bunning, T. J. *Macromolecules* **2004**, *37*, 3792.
(55) Fukuda, J. *Phys. Rev. E* **1999**, *59*, 3275.
(56) Krausch, G.; Dia, C.; Kramer, E. J.; Marko, J. F.; Bates, F. S. *Macromolecules* **1993**, *26*, 5566.
(57) Matsuyama, A.; Kato, T. *J. Chem. Phys.* **1998**, *108*, 2067.
(58) Strobl, G. *The Physics of Polymers*, 2nd ed.; Springer: Berlin, 1997.
(59) Jones, R. A.; Norton, L. J.; Kramer, E. J.; Bates, F. S.; Wiltzius, P. *Phys. Rev. Lett.* **1991**, *66*, 1326.
(60) Shin, K.; Xiang, H. Q.; Moon, S. I.; Kim, T.; McCarthy, T. J.; Russell, T. P. *Science* **2004**, *306*, 76.
(61) Vorflusev, V.; Kumar, S. *Science* **1999**, *283*, 1903.

MA0527045